PAPER

Check for updates

Peroxi-electrocoagulation for treatment of trace organic compounds and natural organic matter at neutral pH†

Donald R. Ryan,[a] Patrick J. McNamara, [ID][a] Claire K. Baldus,[a] Yin Wang [ID][b] and Brooke K. Mayer [ID] *[a]

Iron-based oxidation technologies can be advantageous for mitigating trace organic compounds (TOrCs) during water and wastewater treatment due to their production of hydroxyl radicals. However, iron-based oxidation often occurs at acidic pH to promote Fenton's reaction, which limits the processes' feasibility for treatment applications. This study focused on utilizing iron-electrocoagulation (EC) paired with *ex situ* H_2O_2 addition (peroxi-electrocoagulation [EC:H_2O_2]) to promote oxidative reactions at neutral pH conditions. The hydroxyl radical probe *para*-chlorobenzoic acid (*p*CBA) was used to gauge oxidant activity and serve as a representative TOrC. The impact of water pH, current density, iron dose, H_2O_2 dose (*i.e.*, [H_2O_2]$_{initial}$/[Fe^{2+}]$_{generated}$ ratio), and the presence of natural organic matter (NOM) were evaluated. Multivariable regressions showed that high levels of H_2O_2 relative to iron (*i.e.*, [H_2O_2]$_{initial}$/ [Fe^{2+}]$_{generated}$ ratio >0.7) inhibited the rate of *p*CBA oxidation, likely due to additional radical quenching from extra H_2O_2. Oxidation of *p*CBA was confirmed at neutral pH conditions, indicating that EC:H_2O_2 may potentially serve as a multi-mechanistic treatment technology capable of oxidation. Experiments were also conducted in real-world water samples to gauge EC:H_2O_2 applications for treating groundwater, river water, and primary treated wastewater. Overall, H_2O_2 addition enhanced the oxidative degradation of TOrCs while still removing NOM. The one exception was the primary effluent sample, which had the highest degree of oxidant scavenging of all matrices tested. The electrical energy per order (E_{EO}) metric demonstrated that EC:H_2O_2 is competitive with other TOrC oxidation technologies, with the added benefit of NOM mitigation in the same unit process.

Environmental significance

As trace organic compounds are increasingly being monitored in drinking water, technologies are needed that can mitigate their risks. Iron-electrocoagulation paired with hydrogen peroxide can potentially serve as an oxidative technology for these contaminants, and can simultaneously remove trace organics and bulk organics such as natural organic matter within the same unit process. This combined process can be particularly advantageous for rural and decentralized systems due to multiple treatment processes occurring within the same reactor and favorable energy requirements as compared to oxidation technologies such as UV-H_2O_2 and ozonation.

1. Introduction

Iron has expansive applications for water and wastewater treatment. Different iron-based treatment pathways proceed depending on the valence state of the iron (*e.g.*, ferrous [Fe^{2+}] or ferric [Fe^{3+}]). Iron speciation varies as a function of pH and the presence of dissolved oxygen in water. Ferric iron predominates

in the oxygen-rich neutral and basic pH conditions that are typical for water and wastewater treatment. During coagulation, iron is dosed as ferric chloride or ferric sulfate targeting removal of turbidity and natural organic matter (NOM).[1] Alternately, Fe^{2+} predominantly exists in acidic conditions, and can mediate oxidative treatment *via* Fenton's reaction, which produces hydroxyl radicals (HO˙) that can oxidize trace organic compounds (TOrCs).[2–4] Accordingly, iron-based treatments typically feature either non-destructive removal or oxidative destruction due to dominant pathways under different pH conditions.[5] Research is needed to simultaneously promote both non-destructive and oxidative destructive pathways through Fenton's reaction at circumneutral pH for treating multiple classes of contaminants such as bulk organics (*i.e.*,

[a]Department of Civil, Construction and Environmental Engineering, Marquette University, Milwaukee, WI 53233, USA. Tel: +414-288-2161. E-mail: Brooke.Mayer@marquette.edu

[b]Department of Civil and Environmental Engineering, University of Wisconsin-Milwaukee, Milwaukee, WI 53201, USA

† Electronic supplementary information (ESI) available. See DOI: https://doi.org/10.1039/d3va00138e

NOM) and TOrCs in a single unit process, which can be beneficial for water and wastewater treatment facilities.

Fenton's reaction relies on non-complexed Fe^{2+} and H_2O_2 as reagents to form $HO^•$ (Reaction 1, Table 1). Hydroxyl radicals are highly reactive (2.8 V *vs.* standard hydrogen electrode) and can react with Fenton's reagents (Reactions 4 and 5) at faster rates (10^8 M^{-1} s^{-1}) than the radicals are generated (40–80 M^{-1} s^{-1}), which terminates Fenton's reaction due to oxidant and reagent depletion and hinders treatment effectiveness. However, in acidic conditions (pH 2–4), soluble Fe^{3+} can be recycled into Fe^{2+} (Reaction 2), thereby continuing $HO^•$ generation without reagent depletion.

At neutral pH conditions in water and wastewater treatment, the feasibility of Fenton's reaction is limited for several reasons:

1. Iron speciation shifts toward Fe^{3+}, which is less soluble and more prone to floc formation compared to Fe^{2+}, resulting in termination of the Fenton's reaction cycle by inhibiting regeneration of Fe^{2+} required for oxidant generation.

2. Dissolved oxygen readily oxidizes Fe^{2+} in neutral and basic pH conditions (Reaction 3). Each increase in pH unit increases the oxidation rate of Fe^{2+} 100-fold, leading to less available Fenton's reagents.[9,10]

3. Anionic ligands in natural waters (*e.g.*, OH^- and CO_3^{2-}) form complexes with Fe^{2+}, which decreases the amount of non-complexed Fe^{2+} available to react with H_2O_2 to generate oxidants.[6]

Accordingly, pH limitations restrict Fenton applications to a narrow pH range (pH 2–4), which impedes implementation in water and wastewater treatment due to the intensive pH adjustments to acidify and neutralize waters before and after treatment. Additionally, acidic waters can enhance corrosion of infrastructure and shift the pH of natural waters following discharge.[6]

To facilitate Fenton oxidation at neutral pH, the key premise relies on generating or stabilizing the Fe^{2+} needed to react with H_2O_2 to form $HO^•$. Accordingly, electrochemical water treatment processes, such as electrocoagulation (EC), may be used for Fenton oxidation at neutral pH by generating non-complexed Fe^{2+} *via* anodic dissolution of iron electrodes.[11]

Continuous generation of Fe^{2+} can be advantageous for Fenton oxidation at neutral pH by minimizing the need for Fe^{3+} reduction to Fe^{2+} *via* H_2O_2 (Reaction 2). Prior research has also shown that EC alone can generate $HO^•$ to treat TOrCs through the *in situ* generation of Fe^{2+} at the anode and H_2O_2 production at the cathode.[12–14] During electrolysis, the microenvironment near the anode surface is acidic.[15] Consequently, Fenton reactions may occur at the vicinity of the anode surface even if the bulk solution pH is circumneutral, potentially leading to oxidative conditions at neutral pH between H_2O_2 and the iron anode surface. Supplemental addition of H_2O_2 as a radical promotor, known as peroxi-electrocoagulation (EC:H_2O_2), can further enhance EC's oxidizing capacity and serve as a multi-mechanistic process. During EC:H_2O_2, Fe^{2+} is continually generated at low concentrations (nM s^{-1} based on Faraday's law) over the course of electrolysis, such that non-complexed Fe^{2+} is available for oxidation by H_2O_2. As a result, less Fe^{2+} is "wasted" as a Fenton's reagent by non-radical generating side reactions such as ligand complexation or oxygenation.[11] This combination of Fe^{2+} reagent generation and minimal reliance on Fe^{3+} reduction to Fe^{2+} can make EC:H_2O_2 an advantageous dosing method compared to *ex situ* reagent dosing in Fenton applications. Of note, while *in situ* Fe^{2+} dosing can be advantageous, *ex situ* H_2O_2 dosing may still be needed, depending on EC:H_2O_2 reactor design.

Pratap and Lemley (1998, 1994)[8,16] demonstrated point-of-concept use of EC:H_2O_2 for remediation of the herbicides atrazine and metalochlor at neutral pH conditions. Since the inception of EC:H_2O_2, research has primarily focused on coagulation/flocculation during industrial wastewater treatment for removing bulk organic pollutants (such as chemical oxygen demand) at high concentrations (mg L^{-1} levels).[5,17–22] However, these high-strength wastewater studies do not translate well to municipal wastewater and drinking water treatment applications. For example, environmental waters have lower conductivity, fewer oxidant scavengers, higher dissolved oxygen, and neutral pH conditions, all of which impact the oxidative efficiency of EC:H_2O_2 and speciation of iron in water. Considering iron's treatment capabilities, EC:H_2O_2 may also

Table 1 Fenton's reaction. Iron species are color-coded to reflect the valence state: blue represents ferrous iron (Fe^{2+}) and orange represents ferric iron (Fe^{3+})[a]

Reaction	Chemical reaction	Role
1	$Fe^{2+} + H_2O_2 \rightarrow Fe^{3+} + HO^• + OH^-$	Radical production
2	$Fe^{3+}_{(aq)} + H_2O_2 \rightarrow Fe^{2+} + HO_2^• + H^+$	Ferrous regeneration *via* ferric reduction
3	$Fe^{2+} + \frac{1}{4}O_2 + 2OH^- + \frac{1}{2}H_2O \rightarrow Fe(OH)_{3\,(s)}$	Oxygenation of ferrous iron, reagent quenching
4	$Fe^{2+} + HO^• \rightarrow Fe^{3+} + OH^-$	Radical quenching, reagent quenching
5	$H_2O_2 + HO^• \rightarrow HO_2^• + H_2O$	Radical quenching, reagent quenching

[a] Reactions adapted from ref. 2, 3 and 6–9.

© 2023 The Author(s). Published by the Royal Society of Chemistry

Environ. Sci.: Adv., 2023, **2**, 1574–1586 | **1575**

offer an opportunity for simultaneous treatment of TOrCs and bulk organics (*e.g.*, NOM and chemical oxygen demand) in a single unit process as the Fe^{3+} produced following Fenton's reaction can subsequently contribute to physical removal (*i.e.*, non-destructive removal) of contaminants through coagulation, flocculation, and sedimentation processes.

The goal of this research was to evaluate $EC:H_2O_2$ for simultaneous treatment of both TOrCs and NOM at neutral pH conditions. To vet oxidation, *para*-chlorobenzoic acid (*p*CBA) was selected as the representative TOrC, and also served as a $HO^{\bullet}$ probe for advanced oxidation process (AOP) effectiveness.[23] The relative impacts of current density (*i.e.*, iron dosing rate), H_2O_2 dose, and the corresponding $[H_2O_2]_{initial}/[Fe^{2+}]_{generated}$ ratio were tested in synthetic matrices. Experiments were conducted to differentiate non-destructive removal *via* EC-only from oxidative destructive removal and to assess the contribution of potential oxidants generated in $EC:H_2O_2$ such as $HO^{\bullet}$ and H_2O_2. Experiments were also conducted using surface water, groundwater, and wastewater sources to evaluate the influence of water quality parameters (*i.e.*, dissolved organic carbon [DOC], pH, conductivity, and ions) and the feasibility of $EC:H_2O_2$ for different treatment applications. Finally, electrical energy per order of magnitude reduction (E_{EO}) was calculated for all matrices to provide a means of comparing $EC:H_2O_2$ energy requirements relative to other advanced oxidation processes.

2. Materials and methods

2.1. Experimental protocols for $EC:H_2O_2$ tests of *p*CBA removal

The $EC:H_2O_2$ batch experiments were conducted for 15 minutes of electrolysis with 150 rpm mixing ($G = 180$ s^{-1}) in 4 mM HCO_3^- buffer solutions containing 400 μg L^{-1} *p*CBA. The *p*CBA concentration of 400 μg L^{-1} was selected based on reliable analytical quantification of >90% removal at a target *p*CBA concentration below that of mg L^{-1}-level background oxidant scavengers (*i.e.*, NOM). Electrolysis was performed in 200 mL polypropylene beakers using 1020 steel iron electrodes (VMetals, Milwaukee, WI), which were sanded and wet polished with 320 grit silicon carbide sandpaper prior to experiments. An XPH 75-2D Dual DC power supply (Sorenson Electronics, Cedar City, UT) was used to carry out electrolysis at currents ranging from 40 mA to 200 mA through a submerged electroactive surface area of 13.5 cm^2, as described in Ryan *et al.* (2020).[24] The power supply was equipped with a polarity reversal device to alternate the anode and cathode every 30 seconds based on prior works.[25] For evaluating oxidative treatment, *p*CBA (99%, Sigma Aldrich, St. Louis, MO) was selected as the $HO^{\bullet}$ probe due to its resistance to sorption on iron flocs and frequent use as a radical probe to demonstrate the treatability of TOrCs by $HO^{\bullet}$ exposure.[23,26–28] Compared to other TOrCs, *p*CBA is classified as having "moderate reactivity" with $HO^{\bullet}$, as reported by Gerrity *et al.* (2012),[23] which is similar to TOrCs of concern such as atrazine and 1,4-dioxane.[23]

Three reactor inputs – current density, H_2O_2 dose, and the corresponding $[H_2O_2]_{initial}/[Fe^{2+}]_{generated}$ ratio – were evaluated

to gauge their relative influence on treatment. For EC experiments, the current density was synonymous with the iron loading rate. The iron applied in each test was varied by adjusting the current density (and consequently the iron loading rate). For these experiments, the current density ranged from 3 to 15 mA cm^{-2} (charge loading rate = 12–60 Coulomb L^{-1} min^{-1}, iron loading rate = 3.5–17.3 mg-Fe^{2+} per L-min). The H_2O_2 stock (ACS reagent grade, Sigma Aldrich, St. Louis, MO) was added at the beginning of $EC:H_2O_2$ experiments at levels ranging from 10 to 200 mg H_2O_2 per L to assess *p*CBA treatment resulting from a fixed amount of H_2O_2 available for Fe^{2+} to generate radicals. The corresponding $[H_2O_2]_{initial}/[Fe^{2+}]_{generated}$ was 0.3–1.6 based on current density and H_2O_2 inputs. Notably, the $[H_2O_2]_{initial}/[Fe^{2+}]_{generated}$ ratio reflects the total H_2O_2 added at the beginning of the reaction, divided by the amount of Fe^{2+} generated by EC (estimated by Faraday's Law) by the end timepoint when *p*CBA removal ceased due to H_2O_2 depletion. The end timepoint of the *p*CBA degradation reaction was determined as the time point at which less than 10% difference in *p*CBA removal compared to the preceding time point was observed, likely indicating depletion of H_2O_2. Samples were collected every 2.5 minutes for 10 minutes, with a final sample at 15 minutes for kinetic analyses. Kinetic curves were fit to at least four data points ($R^2 > 0.95$ for all) to calculate first order rate constants for *p*CBA degradation for samples collected prior to H_2O_2 depletion, assessed as noted above.

2.2. Removal pathway control experiments

Experiments were conducted under the same electrolysis and current density conditions described in Section 2.1 to isolate the impact of different system inputs and delineate the potential treatment pathways in $EC:H_2O_2$, including oxidation by $HO^{\bullet}$ and H_2O_2 as well as physical removal by sorption to iron flocs. For $HO^{\bullet}$ oxidation controls, methanol was spiked in stoichiometric excess (12 mM MeOH) of *p*CBA and H_2O_2 to quench $HO^{\bullet}$ that would otherwise react with *p*CBA. In this case, H_2O_2 is reactive with electron-dense compounds and unlikely to react with unsaturated alcohols such as methanol. For no electricity controls (*e.g.*, H_2O_2 controls), 30 mg-H_2O_2 per L was spiked into the reactors containing the iron electrodes and stirred for 15 minutes to assess the potential *p*CBA removal due to H_2O_2 under treatment conditions without electricity in addition to potential losses *via* sorption to the electrode surface.

Kinetic analyses were conducted to estimate the competition between H_2O_2 and O_2 as a function of H_2O_2 inputs and water chemistry conditions (H_2O_2 dose, O_2, and pH). These tests assessed the feasibility of $HO^{\bullet}$ generation under neutral pH conditions and informed mechanistic analyses (oxidation by O_2 limits $HO^{\bullet}$ production by generating Fe^{3+}). The relative rates of oxidation and associated rate constants are provided in the ESI S4.†

2.3. Water quality conditions

All $EC:H_2O_2$ experiments were conducted in 4 mM bicarbonate solution (with the exception of the environmental waters) to simulate buffered conditions for neutral pH environmental

1576 | *Environ. Sci.: Adv.*, 2023, **2**, 1574–1586

© 2023 The Author(s). Published by the Royal Society of Chemistry

Table 2 Water quality parameters

Water matrix	Initial pH	H_2O_2 demand,[a] mg L^{-1} (% H_2O_2 removal)	DOC, mg-C per L	Alkalinity, mg L^{-1} as $CaCO_3$	Conductivity, $\mu S\ cm^{-1}$	Ca^{2+}, mg L^{-1}	Mg^{2+}, mg L^{-1}
Bicarbonate buffer[b]	8.3[c]	0 (0%)	0, 7.5[d]	210	370[e]	0	0
Groundwater	7.30	10 (33%)	3.3	400	1430	70	40
River water	8.4	5 (15%)	7.0	240	755	30	20
Primary wastewater effluent	7.1	23 (75%)	55	280	1400	40	15

[a] H_2O_2 demand is reported as the decrease in H_2O_2 concentration after 15 minutes (the length of batch experiments), where the initial concentration was 30 mg L^{-1} H_2O_2. [b] All model waters were prepared in Milli-Q water with 4 mM HCO_3^-. [c] pH varied from 3 to 10.3 depending on the experiment. The unadjusted pH was 8.3. [d] For NOM tests, NOM was added as International Humic Substance Society Suwannee River NOM. [e] Conductivity varied for pH tests due to the addition of acid (HCl) or base (NaOH) for pH adjustment. At pH 3, conductivity = 920 $\mu S\ cm^{-1}$. At pH 6.3, conductivity = 450 $\mu S\ cm^{-1}$. At pH 10.3, conductivity = 750 $\mu S\ cm^{-1}$. For unadjusted pH, conductivity = 370 $\mu S\ cm^{-1}$.

waters containing alkalinity, and to supply an electrolyte for electrochemical reactions (Table 2). Environmental waters were sampled to assess the impact of water quality and treatment performance in real waters relative to synthetic waters containing different NOM sources (Table 2). These analyses are important for informing the role of other environmentally relevant water quality parameters such as NOM characteristics and concentration, conductivity, and divalent cations, all of which can impact treatment efficacy. A sample from the Milwaukee River (Milwaukee, WI) was used to test the impact of NOM and mid-range conductivity water. Groundwater from a drinking water well in West Bend, WI, was tested to reflect low dissolved organic carbon (DOC) and high conductivity conditions. Finally, primary effluent from an urban water reclamation facility in Milwaukee, WI, was tested for the impact of high DOC due to anthropogenic NOM and other oxidant scavengers (such as bulk chemical oxygen demand). The wastewater also served as a point of comparison to previous EC:H_2O_2 wastewater studies. For DOC quantification experiments, a sedimentation phase was required after EC:H_2O_2 to allow the flocs to settle prior to DOC analysis. Batch tests were performed as described in Section 2.1 followed by an additional tapered flocculation phase (10 minutes at 40 rpm [$G = 25\ s^{-1}$] and 10 minutes at 20 rpm [$G = 9\ s^{-1}$]) and a 20 minute sedimentation period to remove flocs (method adapted from Ryan et al. (2020)).[24]

2.3.1. Analytical measurements. Liquid chromatography-mass spectrometry was utilized to quantify pCBA (method adapted from Vanderford et al. (2007)[28]). All pCBA samples were filtered through 0.22 μm PTFE syringe filters (Agela Technologies, Wilmington, DE) prior to analyses. Additional information on chromatography and mass spectrometry conditions is provided in ESI S1.† The H_2O_2 concentrations before and after each experiment were measured using Hach Model Hyp-1 test kits. The DOC was measured via a Shimadzu TOC – V_{CSN} based on U.S. EPA Method 415.3. All DOC samples were filtered through 0.45 μm PTFE filters (Agela Technologies) prior to analyses. ICP-MS (7700 series, Agilent Technologies, Santa Clara, CA) was used to measure cations in real-world water samples. Alkalinity was measured via titration using Hach Model 2443-89 test kits.

2.3.2. Electrical energy per order. Electrical energy per order of magnitude removal (E_{EO}), as shown in eqn (1), was estimated to provide a figure of merit for comparing energy requirements (kW h m^{-3}-order) for EC:H_2O_2 to other oxidative treatment technologies.[29] The voltage reading was recorded for each current density during each test to calculate power (power = voltage × current). Pseudo-first order rate constants were used to normalize treatment times across experiments as different reactor inputs and water quality conditions required different treatment times for 90% pCBA removal.

$$E_{EO} = \frac{P}{V \times 0.4343k \times 3600 \times 1000} \quad (1)$$

where P is power in W, V is volume in m^3, and k is the pseudo-first order rate constant for pCBA removal in s^{-1}. The coefficient of $0.4343 = \log(C_0/C_i)$ for one order of magnitude reduction. The conversion factor 3600 is used to convert seconds to hours, and 1000 is used to convert W to kW.

2.3.3. Data analysis and interpretation. GraphPad Prism (version 9.5.1.) software was used to conduct one-way and two-way ANOVA followed with Tukey's multiple comparison post-hoc test, Pearson correlations, and multivariable linear regressions. Multivariable linear regressions were used as explanatory models to evaluate the contributions of system inputs (H_2O_2, Fe^{2+}, and $[H_2O_2]_{initial}/[Fe^{2+}]_{generated}$) and the impact of water quality parameters. Independent variables for the EC:H_2O_2 process were selected based on Pearson correlations and normalized using the min-max method. This min-max normalization method was conducted to minimize the artificial impacts of independent variables on the dependent variable due to different scales and ranges of inputs (e.g., rate constants were on the order of $10^{-4}\ s^{-1}$, whereas H_2O_2 ranged from 10 to 100 mg L^{-1}).[30] The independent variables for reactor inputs (pH, $[H_2O_2]_{initial}/[Fe^{2+}]_{generated}$, and current density) were selected for the multivariable linear regression model based on their correlation to the dependent variables: pCBA removal, pseudo-first order rate constant, and E_{EO}. For environmental waters, $DOC_{initial}$, alkalinity, pH, and conductivity were selected as the independent water quality variables. All independent variables selected for multivariable linear regression were not multicollinear with other variables based on variance inflation factors <5 for all regressions.[31]

3. Results and discussion

3.1. *Para*-chlorobenzoic acid removal for hydroxyl radical validation

Removal of *p*CBA during EC:H$_2$O$_2$ primarily proceeded *via* oxidation at neutral pH conditions due to the system's combination of iron and H$_2$O$_2$ (Fig. 1). EC-only controls yielded an average *p*CBA removal of approximately 15%, presumably due to the low levels of HO$^•$ that can be generated during EC alone.[13,14] For EC:H$_2$O$_2$ + MeOH experiments, the high MeOH concentration (12 mM) scavenged the oxidants and resulted in negligible *p*CBA degradation. This scavenging indirectly underscores the role of homogeneous oxidants (such as HO$^•$). Negligible *p*CBA removal in the EC:H$_2$O$_2$ + MeOH test further indicates that *p*CBA does not sorb to iron flocs. The 'No Electricity Control' experiments demonstrated that potential reactions between H$_2$O$_2$ and the iron electrode surface had minimal removal relative to the EC:H$_2$O$_2$ conditions with electricity ($p <$ 0.0001, one-way ANOVA) at circumneutral pH conditions. Overall, these data demonstrate that the addition of H$_2$O$_2$ can enhance oxidant production in EC:H$_2$O$_2$ relative to EC alone and induce oxidative processes at neutral pH conditions.

The occurrence of oxidation at neutral pH conditions during EC:H$_2$O$_2$ is important in the context of Fenton literature since traditional Fenton oxidation proceeds at highly acidic pH 3 conditions. These conventional Fenton conditions limit the feasibility of EC:H$_2$O$_2$ applications as the high acidity can damage infrastructure, enhance corrosion, and incur chemical costs for acidifying and neutralizing water during treatment.

3.2. The impact of reactor inputs on *p*CBA degradation during EC:H$_2$O$_2$: removal and kinetics

Following oxidant verification, the impact of EC:H$_2$O$_2$ reactor inputs and water quality were assessed. The discussion centers on the role of [H$_2$O$_2$]$_{initial}$/[Fe^{2+}]$_{generated}$ ratios, current density, and pH. Multivariable linear regressions were used to parameterize the contribution of all inputs.

3.2.1. The impact of H$_2$O$_2$ dose, current density, and iron dose on *p*CBA removal at neutral pH conditions. The efficacy of H$_2$O$_2$ dose for *p*CBA removal varied as a function of the [H$_2$O$_2$]$_{initial}$/[Fe^{2+}]$_{generated}$ ratio (Fig. 2A). The presence of H$_2$O$_2$ only improved treatment when Fe^{2+} was also present in the system ($R_{H_2O_2\text{-all:removal}}^2 = 0.003$, $p = 0.99$ Pearson correlation, Table S13†). With 10–40 mg L^{-1} H$_2$O$_2$, there was a positive correlation between *p*CBA removal and H$_2$O$_2$ dose during EC:H$_2$O$_2$ when iron was also present in the system ($R_{H_2O_2\text{:removal}}^2 = 0.84$, $p < 0.05$ Pearson correlation, Table S14†). Once H$_2$O$_2$ exceeded 30 mg L^{-1} in the presence of Fe^{2+}, *p*CBA removal began to plateau around 50–60% *p*CBA removal for [H$_2$O$_2$]$_{initial}$/[Fe^{2+}]$_{generated}$ ratios ranging from 0.3 to 0.7. In contrast, the higher [H$_2$O$_2$]$_{initial}$/[Fe^{2+}]$_{generated}$ ratio of 1.6 resulted in less *p*CBA removal compared to the same H$_2$O$_2$ dose applied at lower ratios. Alternately, for H$_2$O$_2$ concentrations greater than 40 mg L^{-1}, the H$_2$O$_2$ dose did not significantly correlate ($R_{H_2O_2>40\text{:removal}}^2 = -0.377$, $p = 0.136$, Pearson correlation, Table S15†) and resulted in less *p*CBA removal. For example, 50 mg L^{-1} H$_2$O$_2$ had approximately 60% *p*CBA removal when applied at [H$_2$O$_2$]$_{initial}$/[Fe^{2+}]$_{generated}$ = 0.35; when the ratio increased to [H$_2$O$_2$]$_{initial}$/[Fe^{2+}]$_{generated}$ = 1.6, *p*CBA removal decreased to 40% for all H$_2$O$_2$ doses. The inhibition of *p*CBA removal at higher H$_2$O$_2$ levels aligns with the scavenging impact of H$_2$O$_2$ and competition between matrix constituents. Although more H$_2$O$_2$ can be beneficial for HO$^•$ generation *via* Fenton's reaction, higher H$_2$O$_2$ levels lead to a higher degree of oxidant scavenging and decreased radical availability for *p*CBA removal (ESI S3).†

The key role of current density in this study was to adjust the iron loading rate to add Fe^{2+} as Fenton's reagent (Fig. 2B). When no H$_2$O$_2$ was present (*i.e.*, EC-only), *p*CBA removal was consistently less than 20% regardless of current density (Fig. 2C). Hence, EC offered effective *p*CBA removal only when H$_2$O$_2$ was present, indicating that the [H$_2$O$_2$]$_{initial}$/[Fe^{2+}]$_{generated}$ ratio was the key driver of treatment efficacy. During EC:H$_2$O$_2$, *p*CBA removal improved with increases in current density up to 7.4 mA cm^{-2} ($R_{current\ density=3\ to\ 7.4\ mA\ cm^{-2}}^2 = 0.63$, $p = 0.008$,
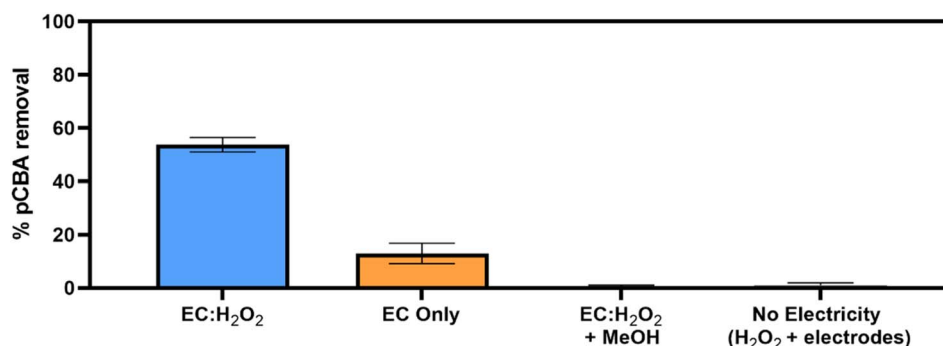

Fig. 1 Mechanisms for *p*CBA removal during EC:H$_2$O$_2$ at 7.40 mA cm^{-2}. A series of controlled batch experiments were run in 4 mM bicarbonate buffer at pH 8.3 for 15 minutes. In "EC only," electrolysis was conducted using iron electrodes with no peroxide addition. For "EC:H$_2$O$_2$ + MeOH", methanol was spiked in stoichiometric excess of *p*CBA (12 mM MeOH:2.5 µM *p*CBA) to quench oxidants that would otherwise degrade *p*CBA. In "No Electricity (H$_2$O$_2$ + electrodes)", 30 mg L^{-1} H$_2$O$_2$ was spiked into the solution with the iron electrodes and mixed for 15 minutes. All experiments were conducted in duplicate and error bars indicate ± 1 standard deviation. EC-only results are the average of all duplicate experiments for each EC-only control, including current densities of 3.5 mA cm^{-2}, 5.5 mA cm^{-2}, 11.1 mA cm^{-2}, and 15 mA cm^{-2}, where $n = 8$.
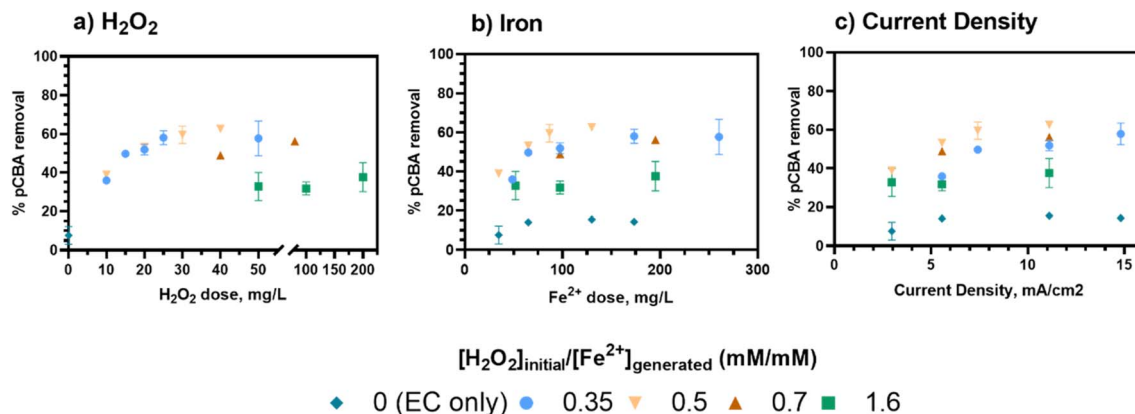
Fig. 2 pCBA removal after 15 minute EC:H_2O_2 batch experiments as a function of (a) H_2O_2 initially dosed into the system, (b) total ferrous iron generated (estimated by Faraday's law) over the course of the EC:H_2O_2 experiment, and (c) current density, which is proportional to the iron loading rate (mg-Fe per L). Iron loading rates were estimated using Faraday's law, where 3 mA cm^{-2} = 3.5 mg-Fe per L-min, 5.5 mA cm^{-2} = 6.5 mg-Fe per L-min, 7.4 mA cm^{-2} = 8.6 mg-Fe per L-min, 11.1 mA cm^{-2} = 13 mg-Fe per L-min, and 15 mA cm^{-2} = 17.4 mg-Fe per L-min. All experiments were conducted in duplicate and error bars indicate $\pm$ 1 standard deviation.

Pearson correlation, Table S16†) and plateaued after 7.4 mA cm^{-2} ($R_{\text{current density}>7.4\text{ mA cm}^{-2}} = 0.141$, $p = 0.6$, Pearson correlation). As treatment inputs increased, the higher ratio of [H_2O_2]$_{\text{initial}}$/[Fe^{2+}]$_{\text{generated}}$ = 1.6 had the least pCBA removal for EC:H_2O_2 regardless of current density. The plateau in pCBA removal for higher current density may suggest that a minimum level of iron is needed for this system, and beyond that level, additional iron no longer improves treatment. Here, the lowest Fe^{2+} loading rate was 3.5 mg Fe per L-min (resulting from 3 mA cm^{-2} current density).

In summary, [H_2O_2]$_{\text{initial}}$/[Fe^{2+}]$_{\text{generated}}$ ratios were the key driver for pCBA removal where lower ratios (0.33–0.7) had higher removal ($\beta_{\text{H}_2\text{O}_2/\text{Fe}=0-0.7} = 0.77$, $p < 0.0001$, multivariable linear regression: "% R, low ratio, neutral pH") from minimal HO˙ scavenging, and higher ratios (1.6) decreased removal ($\beta_{\text{H}_2\text{O}_2/\text{Fe}=0.3-1.6} = -0.42$, $p = 0.0008$, multivariable linear regression: "% R EC: H_2O_2 neutral pH"). This finding is important when considering material requirements including the *ex situ* H_2O_2 additions and the power demands associated with iron generation. For this system, H_2O_2 levels determined the treatment capacity because pCBA removal ceased after depletion of the one-time dose of H_2O_2 at the start of the test, whereas the Fe^{2+} was continually generated *via* electrolysis.

It is important to note that [H_2O_2]$_{\text{initial}}$/[Fe^{2+}]$_{\text{generated}}$ ratios do not translate to the actual ratio of H_2O_2 relative to Fe^{2+} at any timepoint during the test. During EC:H_2O_2, H_2O_2 is initially in large excess to Fe^{2+} as Fe^{2+} is formed during EC, which may drive the rate of oxidant formation resulting from interactions between Fe^{2+} and H_2O_2. This excess is a result of Fe^{2+} being generated at nM levels (*e.g.*, 2500 nM s^{-1} for 7.4 mA cm^{-2} based on Faradays law) during electrolysis, which highlights the benefits of using iron electrolysis for Fe^{2+} dosing to avoid side reactions and encourage efficient Fe^{2+} utilization by H_2O_2.

3.2.2. The impact of [H_2O_2]$_{\text{initial}}$/[Fe^{2+}]$_{\text{generated}}$ and current density on pCBA oxidation rate during EC:H_2O_2. Pseudo-first order kinetic modeling offered good data fits, enabled comparison to other AOP processes in the literature, and was

used in E_{EO} calculations. For a fixed current density of 5.5 mA cm^{-2}, [H_2O_2]$_{\text{initial}}$/[Fe^{2+}]$_{\text{generated}}$ = 0.35, 0.5, and 0.7 had similar pseudo-first order rate constants (1.1×10^{-3} to 1.3×10^{-3} s^{-1}) before H_2O_2 depletion (Fig. 3A and Table S5†). As the ratio increased, the rate of pCBA removal declined, which corroborates the removal findings in Section 3.2.1. Notably, for [H_2O_2]$_{\text{initial}}$/[Fe^{2+}]$_{\text{generated}}$ = 0.35 and 0.5, pCBA removal stagnated after 7.5 minutes and 10 minutes, respectively. Accordingly, H_2O_2 should be continually dosed at lower concentrations in EC:H_2O_2 operations in order to continue oxidative reactions without adding excess H_2O_2 that can lead to quenching.

As shown in Fig. 3, for a fixed [H_2O_2]$_{\text{initial}}$/[Fe^{2+}]$_{\text{generated}}$ ratio of 0.5, the rate constants were comparable for current densities of 5.5, 7.4, and 11.1 mA cm^{-2} (1.3 to 1.6×10^{-3} s^{-1}, Table S5†). However, 3 mA cm^{-2} had the lowest rate of removal (8.4×10^{-4} s^{-1}, Table S5†). This trend aligns with the removal data, in which the removal plateaued as current (*i.e.*, iron loading rate) increased, indicating that additional iron after a threshold level no longer improved treatment.

Overall, the ratio had the highest influence on rate of removal based on multivariable linear regressions ($\beta_{[\text{H}_2\text{O}_2]/[\text{Fe}^{2+}]=0-0.77} = 0.76 \pm 0.11$, $p < 0.0001$, multivariable linear regression: "k, EC:H_2O_2 low ratio, neutral pH") (Fig. 3C). Considering both major inputs in terms of [H_2O_2]$_{\text{initial}}$/[Fe^{2+}]$_{\text{generated}}$ ratios, pseudo-first order rate constants were grouped into three clusters for a range of current densities at neutral pH conditions (Fig. 3C) to understand the general impact of different ratio levels. The clusters were EC-only conditions (*i.e.*, no H_2O_2), [H_2O_2]$_{\text{initial}}$/[Fe^{2+}]$_{\text{generated}}$ ratios = 0.3–0.7, and [H_2O_2]$_{\text{initial}}$/[Fe^{2+}]$_{\text{generated}}$ ratios greater than 0.7. The lower [H_2O_2]$_{\text{initial}}$/[Fe^{2+}]$_{\text{generated}}$ ratios of 0.3–0.7 had the highest rate constants, ranging from 1.1×10^{-3} to 1.6×10^{-3} s^{-1}. The higher ratios of >0.7 to 1.6 resulted in lower rate constants, ranging from 5.8×10^{-4} to 7.7×10^{-4} s^{-1} ($\beta_{[\text{H}_2\text{O}_2]/[\text{Fe}^{2+}]=0.3\text{ to }1.6} = -0.59 \pm 0.11$, $p < 0.0001$, multivariable linear regression: "k, EC:H_2O_2 only, neutral pH"). For all cases, experiments containing H_2O_2 had faster rates of pCBA removal compared EC-only controls (1.4×10^{-4} to 2.7×10^{-4} s^{-1}). However, higher levels of H_2O_2 (greater than 40 mg L^{-1})
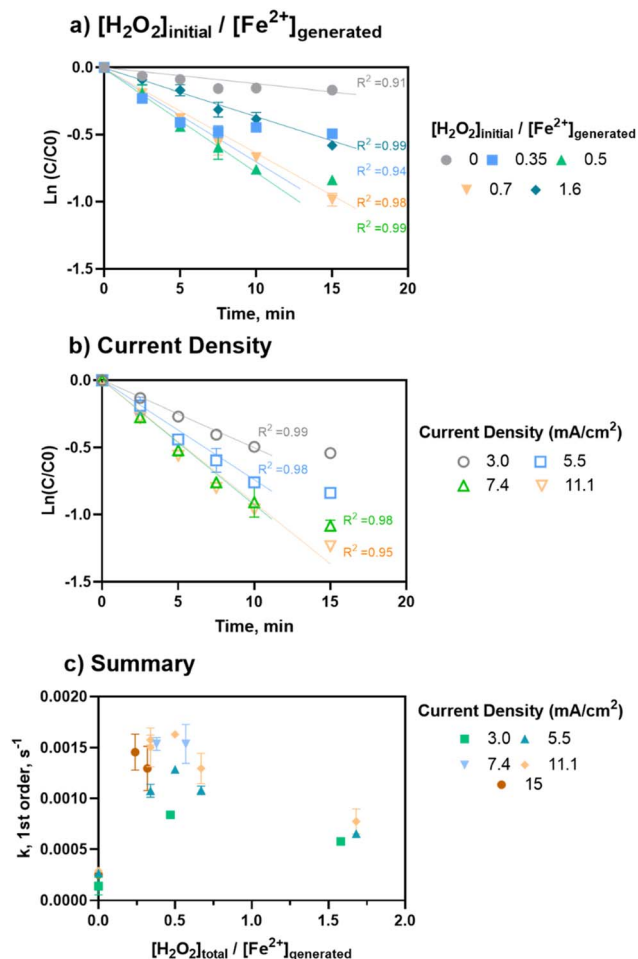
Fig. 3 Summary of pseudo-first order rate constants for degradation of *para*-chlorobenzoic acid (*p*CBA) following 15 minute EC:H_2O_2 batch experiments. All experiments were conducted in 4 mM HCO_3^- buffer at pH = 8.3. Samples were taken every 2.5 minutes for a total of 15 minutes. (a) Pseudo-first order kinetic curves showing the impact of $[H_2O_2]_{initial}/[Fe^{2+}]_{generated}$ ratios for a fixed current density of 5.5 mA cm^{-2}. (b) Pseudo-first order kinetic curves showing the impact of current density for a fixed $[H_2O_2]_{initial}/[Fe^{2+}]_{generated}$ of 0.5. (c) Summary of pseudo-first order rate constants for all EC:H_2O_2 batch experiments for all current density and $[H_2O_2]_{initial}/[Fe^{2+}]_{generated}$ ratios. Pseudo-first order constants were determined and verified based on $R^2 \geq 0.95$ over the course of treatment to capture the linear range prior to H_2O_2 depletion. The end timepoint of the *p*CBA degradation reaction used in kinetic modeling was determined as the time point at which *p*CBA removal was less than 10% different than the preceding time point. Error bars show $\pm$ 1 standard deviation of duplicate experiments.

did not increase the rate of *p*CBA removal, likely due to radical quenching by H_2O_2. This is notable given that the effective H_2O_2 doses found in this study are less than reagent demands in other EC:H_2O_2 studies for industrial treatment applications.[5,17–22] Overall, these findings indicate that less H_2O_2 may be required than previously thought for effective oxidation during EC:H_2O_2.

3.2.3. The impact of pH on oxidation rate. The impact of pH on *p*CBA oxidation was assessed to evaluate the interplay of Fe^{2+}, H_2O_2, and *p*CBA over a range of acid/base conditions. As pH decreased, *p*CBA removal increased and the rate of oxidation

accelerated (Fig. 4). At basic pH 10.3 conditions, minimal removal was observed. At pH 6.3, the maximum rate of *p*CBA degradation was observed (amongst the circumneutral pH levels tested), $k = 4.6 \times 10^{-3}$ s^{-1} (1.6 times faster than the rate at pH 8.3). Removal of *p*CBA ceased after 5 minutes (as indicated by the stagnation of the kinetic curve), likely due to depletion of H_2O_2 at these conditions. Measurements of the H_2O_2 remaining after 5 minutes demonstrated roughly 70% loss of the initial 30 mg L^{-1} H_2O_2 at pH 6.3 and 95% loss at pH 3 (ESI S7†). Depletion of the H_2O_2 helps explain the stagnated *p*CBA removal, likely due to decreased formation of oxidants. Accordingly, H_2O_2 should be continually dosed at lower concentrations in EC:H_2O_2 to encourage continuous oxidative reactions and improve TOrC treatment.

The acidic conditions (pH 3, encouraging Fenton's reactions) resulted in the greatest and fastest *p*CBA removal (>99% removal, to below the detectable limit). However, at pH 3, enhanced corrosivity led to >99% *p*CBA removal even without electricity, wherein increased iron dissolution was visually observed. For no electricity controls, *p*CBA removal was likely due to non-faradaic iron dissolving from the electrodes (30 mg Fe per L) and reacting with *ex situ* H_2O_2 (98% H_2O_2 removal; ESI S7†) to generate HO$^{\bullet}$. The no electricity control resulted in a $[H_2O_2]_{initial}/[Fe^{2+}]_{generated}$ ratio of 1.5. Although this ratio was toward the upper end of ratios tested, the pH 3 conditions were expected to enhance the rate of reaction. For circumneutral conditions, the no-electricity controls had minimal *p*CBA removal, indicating no oxidant generation in the absence of electricity at the conditions tested.

Overall, the *p*CBA removal trends agree with the kinetic modeling performed to estimate the competition between H_2O_2 and O_2 for oxidizing Fe^{2+} (ESI S4†). The modeling scenarios included 0 to 200 mg L^{-1} H_2O_2 concentrations. At pH 6.3, the rate of Fe^{2+} oxidation by H_2O_2 was up to 10 orders of magnitude higher than Fe^{2+} oxidation by O_2, suggesting that there was minimal competition for ferrous oxidation between H_2O_2 and O_2. Accordingly, these kinetic analyses support that HO$^{\bullet}$ generation was driven by Fe^{2+} oxidation *via* H_2O_2 (not O_2). Removal was minimal at pH 10.3, likely due to enhanced O_2 activity (Fig. 4). As pH increases, the inhibition of HO$^{\bullet}$ generation due to O_2 becomes more apparent given that the oxidation of Fe^{2+} by O_2 is second order with respect to $[OH^-]$ (based on Stumm and Lee, 1961[9]) and increases 100-fold for each pH unit increase (ESI S4†).

The pseudo-first order rate constants were used to estimate the HO$^{\bullet}$ concentration (ESI S2†). For pH 8.3, [HO$^{\bullet}$] ranged from 2–4.1 $\times 10^{-13}$ M for the $[H_2O_2]_{initial}/[Fe^{2+}]_{generated}$ ratios of 0.33 to 0.7. At pH 6.3, when *p*CBA treatment was more effective, [HO$^{\bullet}$] was approximately 9 $\times 10^{-13}$ M. These estimates of radical concentrations can be applied to future studies to compare the [HO$^{\bullet}$] yield for a range of TOrC oxidation technologies such as UV/H_2O_2.

3.2.4. Multivariable linear regression analysis of EC:H_2O_2 process inputs. To evaluate the roles of independent variables, multivariable linear regressions were conducted to consider the influence of all reactor input experiments at neutral pH and for variable pH experiments. The key parameters incorporated into
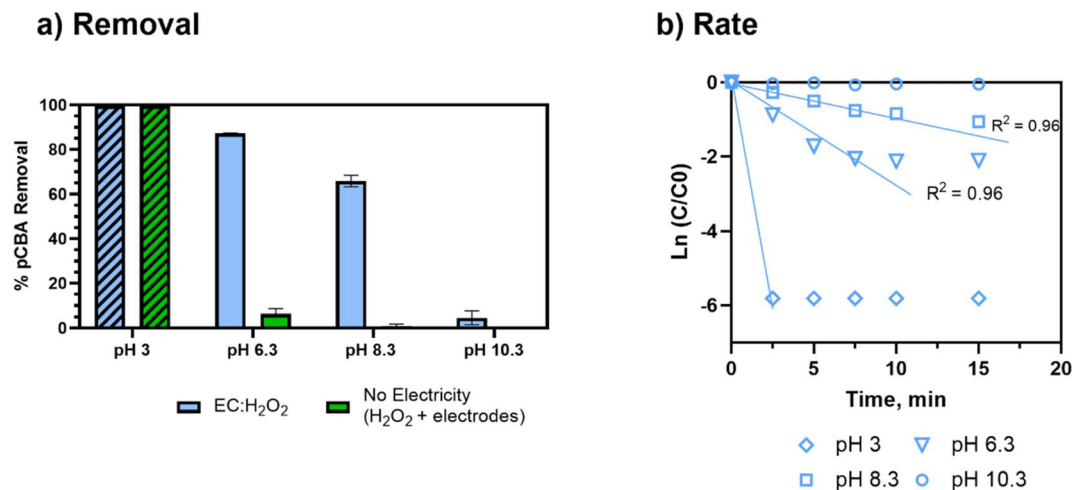
1580 | *Environ. Sci.: Adv.*, 2023, **2**, 1574–1586

© 2023 The Author(s). Published by the Royal Society of Chemistry

Fig. 4 Degradation of pCBA at different pH conditions prepared in 4 mM bicarbonate buffer. During EC:H_2O_2, current density = 7.4 mA cm^{-2}, H_2O_2 = 30 mg L^{-1}, 15 minutes of treatment time. (a) Removal of pCBA as a function of pH. The no electricity control experiment shows removal due only to iron electrodes and the addition of 30 mg L^{-1} H_2O_2. Striped bars indicate concentrations below the limit of detection (4 μg L^{-1}). (b) pCBA removal rate as a function of pH. R^2 correlations are not shown for pH 3 due to insufficient points above the limit of detection after treatment (removal at all pH 3 treatments was calculated using the limit of detection as the final concentration). R^2 is not shown for pH 10.3 due to no removal. The end timepoint of the pCBA degradation reaction used in kinetic modeling was determined as the time point at which pCBA removal was less than 10% different than the preceding time point. Error bars show ± 1 standard deviation of triplicate experiments. Of note, the error bars for b are not visible due to low standard deviation.

the regression were $[H_2O_2]_{initial}/[Fe^{2+}]_{generated}$ ratios, pH, and current density. These independent variables were selected based on preliminary Pearson correlations and were not multicollinear (ESI S6†).

Overall, $[H_2O_2]_{initial}/[Fe^{2+}]_{generated}$ ratios, pH, and current density were significantly correlated to pCBA removal (p = 0.028, 0.008, and <0.0001, respectively, multivariable regression "% R all"). The most influential parameter for pCBA removal was pH ($\beta_{pH} = -0.91 \pm 0.15$, multivariable linear regression: "% R, all"), where lower pH led to higher pCBA removal. The ratio of $[H_2O_2]_{initial}/[Fe^{2+}]_{generated}$ and current density had smaller impacts relative to pH, but similar magnitude of contributions to one another ($\beta_{[H_2O_2]/[Fe^{2+}]} = 0.22 \pm 0.09$, $\beta_{current density} = 0.36 \pm 0.09$, multivariable linear regression: "% R, all").

A separate regression was performed for experiments with $[H_2O_2]_{initial}/[Fe^{2+}]_{generated}$ ratios = 0–0.77 to rank the inputs that yielded higher rate constants and higher pCBA removal. For these tests, pH still had the greatest influence ($\beta_{pH} = -0.79 \pm 0.08$, p < 0.0001, multivariable linear regression: "k, all") followed by $[H_2O_2]_{initial}/[Fe^{2+}]_{generated}$ ratios ($\beta_{[H_2O_2]/[Fe^{2+}]} = 0.38 \pm 0.05$, p < 0.0001, multivariable linear regression: "k, all"). However, variations in current density alone had an insignificant influence on the rate of pCBA removal ($\beta_{current density} = 0.09 \pm 0.05$, p = 0.073, multivariable linear regression: "k, all"), implying that pH and $[H_2O_2]_{initial}/[Fe^{2+}]_{generated}$ ratios are the key parameters influencing oxidant production.

3.3. Co-treatment of pCBA and NOM using EC:H_2O_2 to treat environmental waters and synthetic matrices

3.3.1. pCBA removal in NOM-containing waters. In environmental source waters (*i.e.*, river water and groundwater), EC:H_2O_2 oxidized pCBA, indicating that EC:H_2O_2 can treat real

waters containing relatively low DOC levels typical of natural source waters in addition to synthetic matrices (Fig. 5A). The matrices with the lowest levels of DOC (groundwater and bicarbonate [no DOC]) had similarly high pCBA removal (p = 0.8, ANOVA: post hoc Tukey multiple comparison), whereas the matrices containing moderate DOC levels (river water and SR-NOM) had less pCBA removal and performed similarly to one another (p > 0.99, ANOVA: post hoc Tukey multiple comparison). Notably, the synthetic matrices had similar removal efficacy to the real waters in spite of increased complexity in real water sources.

The initial concentration of DOC had a small impact on pCBA removal ($\beta_{DOC} = -0.07$, p = 0.34, not including primary effluent) for matrices containing low-to mid-range DOC levels (<10 mg-C per L) that reflect drinking water source matrices. This trend implies that the presence of NOM may not heavily impede pCBA oxidation when treating typical environmental source waters.

Compared to real-world waters and synthetic matrices, the primary effluent had the least pCBA removal. Decreased removal was likely due to high H_2O_2 demand (Table 2) and high DOC levels. In this case, the high H_2O_2 demand rapidly depleted the H_2O_2 that was initially dosed into the reactor, which hindered HO$^\bullet$ production. Thus, for EC:H_2O_2 applications, the water's H_2O_2 demand should be accounted for to gauge potential negative impacts on process performance. For example, Serra-Clusellas *et al.* (2021)[32] demonstrated TOrC mitigation *via* EC:H_2O_2 at pH 3 in municipal tertiary treated wastewater containing ng L^{-1} TOrCs by using elevated 220–440 H_2O_2 mg L^{-1} doses (resulting in $[H_2O_2]_{initial}/[Fe^{2+}]_{generated}$ ratios of 1.7 to 2 during treatment), which offset oxidant scavenging by wastewater constituents.
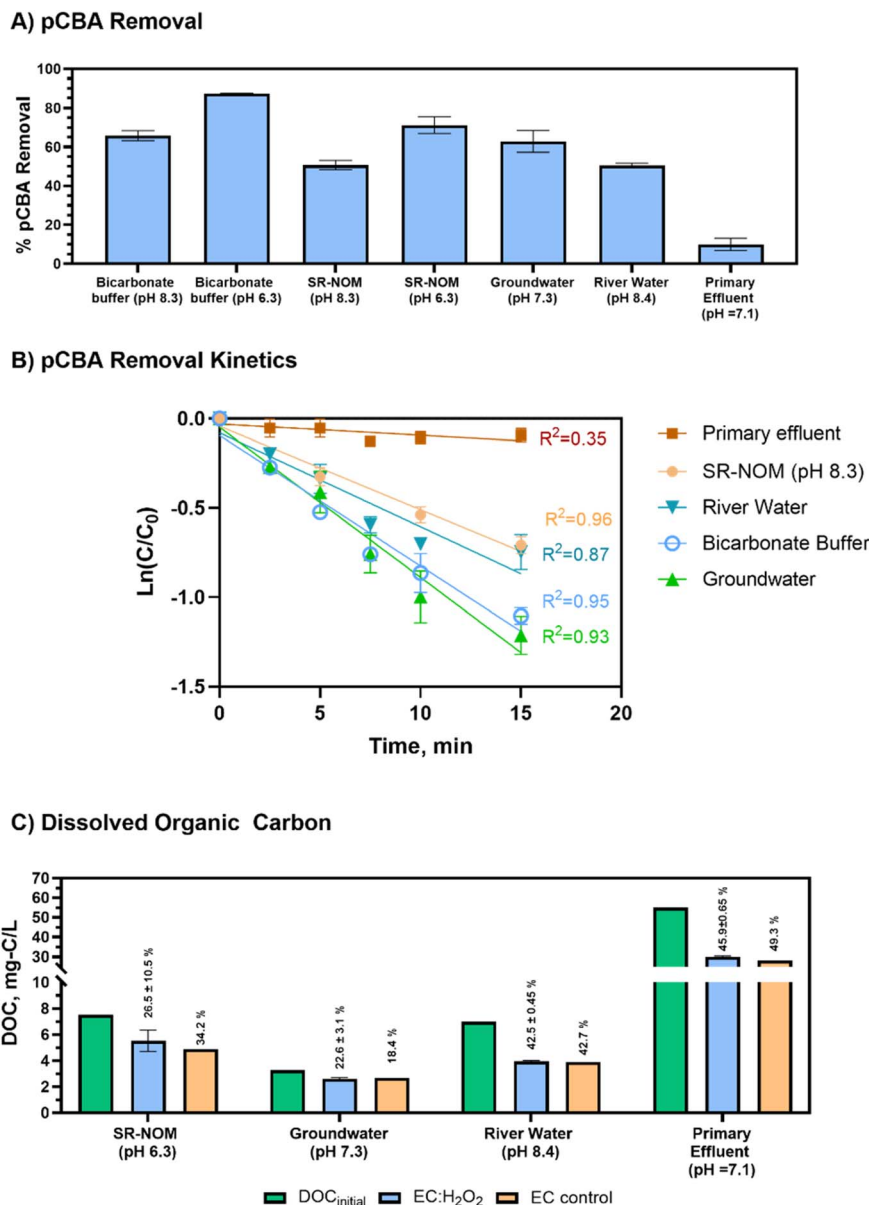
© 2023 The Author(s). Published by the Royal Society of Chemistry

Environ. Sci.: Adv., 2023, **2**, 1574–1586 | **1581**

Fig. 5 Removal of pCBA and dissolved organic carbon (DOC) in synthetic and real-world waters following 15 minutes of EC:H$_2$O$_2$ (7.40 mA cm^{-2}, H$_2$O$_2$ = 30 mg L^{-1}). (A) pCBA removal following EC:H$_2$O$_2$ (C_i = 400 μg L^{-1} for all matrices). (B) Pseudo-first order degradation of pCBA in EC:H$_2$O$_2$ at [H$_2$O$_2$]$_{initial}$/[Fe^{2+}]$_{generated}$ ratio = 0.55 (7.4 mA cm^{-2}, 30 mg H$_2$O$_2$ per L) in synthetic and real-world waters. (C) DOC in the waters initially and remaining following EC:H$_2$O$_2$ or EC-only treatment. A pH 6.3 test was conducted for SR-NOM to reflect enhanced coagulation conditions. Bicarbonate buffer is not included in panel (C) as there was no DOC in the synthetic matrix. The % DOC removal by EC:H$_2$O$_2$ is shown in vertical text above each bar. All DOC and pCBA data are from the same batch experiments for the respective water matrix. Error bars show ± 1 standard deviation of triplicate experiments, with the exception of the "EC control" values in panel C, which are single replicates.

A multivariable regression of all test matrices showed that DOC$_{initial}$ and pH were the key water quality parameters that impacted pCBA removal (β_{DOC} = −0.72 ± 0.18, p = 0.008 and β_{pH} −0.81 ± 0.08, p=<0.0001, respectively). Pearson correlations showed that DOC$_{initial}$ and H$_2$O$_2$ demand were multicollinear ($R_{DOC\ vs.\ H_2O_2\ demand}^2$ = 0.893, p < 0.05, Pearson correlations). As anticipated, higher DOC levels typical of wastewater impeded treatment efficacy, whereas lower DOC conditions improved radical yield and offered less competition for oxidants. However, it is important to note that other water matrix constituents beyond DOC (including chemical oxygen demand, reduced metals, and sulfides, which were not assessed in this study) also likely contributed to H$_2$O$_2$ depletion and impeded DOC removal.

3.3.2. DOC removal in environmental waters. In terms of bulk organics, EC:H$_2$O$_2$ appeared to offer similar levels of DOC removal compared to EC-only, with the added benefit of TOrC mitigation based on pCBA removal (Fig. 5C). The favorable reproducibility of DOC removal *via* EC:H$_2$O$_2$ replicates relative to single EC-only as a point of reference suggests that DOC

removal primarily proceeds through non-destructive pathways as EC-only was previously shown to have minimal pCBA removal *via* oxidants at the conditions tested.

The river water and SR-NOM matrices are of particular interest for DOC removal given that they are representative of surface waters that could be treated for drinking water. Using EC:H$_2$O$_2$, DOC removal for the river water complied with recommendations in the US Environmental Protection Agency's Enhanced Coagulation Guidance manual (>30% DOC removal for matrices containing >120 mg L^{-1} as CaCO$_3$ alkalinity).[33] The synthetic SR-NOM matrix only had effective DOC removal when pH was 6.3. At pH 8.3, EC:H$_2$O$_2$ formed no flocs or precipitates in SR-NOM, indicating unsuccessful coagulation, precipitation, and subsequent sedimentation of flocs (ESI S9†). This difference between real and synthetic waters suggests that other constituents in environmental waters (such as divalent cations, *i.e.*, calcium and magnesium) may improve coagulation processes in real waters by promoting ionic interactions between NOM and ions that promote co-sorption to flocs, as shown for a calcium-fulvic acid-goethite iron mineral system.[34] Overall, the addition of H$_2$O$_2$ during EC:H$_2$O$_2$ can enhance treatment applications by simultaneously treating TOrCs such as pCBA as well as bulk organics such as DOC in a single unit process *in lieu* of a multi-stage treatment train such as coagulation/flocculation/sedimentation followed by filtration and oxidation to achieve both non-destructive removal and oxidative destruction of contaminants.

3.4. Engineering implications: rate constants and electrical energy per order

3.4.1. Pseudo-first order rate constants for treating environmental waters. Pseudo-first order rate constants are key figures of merit for evaluating operational parameters by accounting for matrix-specific scavengers. The pseudo-first order rates for pCBA removal were 1.3×10^{-3} s^{-1} and 1.6×10^{-3} s^{-1} for river water and groundwater, respectively (Fig. 5B and Table 4). These values satisfy the proposed breakeven point $k = 2.1 \times 10^{-5}$ s^{-1} for TOrC treatment technologies to be competitive based on technoeconomic analyses.[35]

3.4.2. Electrical energy per order: impact of reactor inputs assessed in bicarbonate buffer. In terms of energy requirements, higher current densities resulted in higher E_{EO} values ($\beta_{current\ density} = -0.36 \pm 0.09$, $p < 0.0001$, multivariable regression: "E_{EO}, all"), whereas [H$_2$O$_2$]$_{initial}$/[Fe^{2+}]$_{generated}$ ratios had less impact ($\beta_{[H_2O_2]/[Fe^{2+}]} = -0.36 \pm 0.09$, $p = 0.16$). For the lower current densities, 3 and 5 mA cm^{-2}, the E_{EO} was $0.62 \pm$

0.02 and 1.22 ± 0.05 kW h m^3, respectively, when operated at pH 8.3 conditions. The higher current densities of 7.4 to 15 mA cm^{-2} had E_{EO} values ranging from 3.13 ± 0.13 to 12.54 ± 2.12 kW h m^3 due to the additional electrical loading (Table 3). When pH decreased to 6.3, the E_{EO} decreased from 2.86 ± 0.2 kW h m^{-3} to 0.68 ± 0.004 kW h m^{-3} for the same current density of 7.4 mA cm^{-2}. This improvement in energy efficiency was likely due to a combination of the faster rate of removal at pH 6.3 and the solution's increased conductivity due to chloride addition (HCl was used for pH adjustment).

At circumneutral pH, current densities above 3 mA cm^{-2} thus exceeded the recommended 1 kW h m^{-3} E_{EO} threshold to be competitive with conventional HO$^{\cdot}$-mediated advanced oxidation processes (AOPs) such as UV/H$_2$O$_2$ and ozone-based AOPs.[36] Accordingly, EC:H$_2$O$_2$ may be operated at lower current densities for more favorable energy demands. However, the benchmark E_{EO} values for conventional AOPs rely on preliminary treatment technologies such as coagulation and membrane filtration to remove oxidant scavengers, primarily DOC. Additional DOC removal technologies add materials and energy demands to overall treatment of TOrCs that are not accounted for in standalone E_{EO} values for conventional AOPs. Alternately, EC:H$_2$O$_2$ offers the benefit of simultaneous TOrC and DOC treatment, which can minimize preliminary treatment needs and decrease overall energy inputs compared to conventional AOP treatment trains.

Although EC:H$_2$O$_2$ was higher than the E_{EO} benchmark for conventional AOPs under high current conditions, EC:H$_2$O$_2$ generally resulted in a lower range of E_{EO} values (0.6 to 12.5 kW h kW h m^{-3} [Table 3]) compared to pCBA mitigation using other electrochemical technologies such as boron-doped diamond electrooxidation. For example, Lanzarini-Lopes *et al.* (2017)[37] reported E_{EO} values for pCBA mitigation ranging from 39.3 kW h m^{-3} to 332 kW h m^{-3} for electrooxidation current densities from 16.6 to 100 mA cm^{-2}. Consistent with this study, increasing current density in the electrochemical treatment process yielded higher, less favorable E_{EO} values.

3.4.3. Electrical energy per order: impact of water quality. The E_{EO} values for different water matrices ranged from 0.7 to 7.5 kW h m^{-3} (Table 4) as a function of water quality, pCBA removal, and the voltage input to achieve the fixed current of 7.4 mA cm^{-2}. Of the environmental waters, groundwater had the lowest E_{EO} at 1.0 ± 0.13 kW h m^{-3}, while the river water E_{EO} was 1.91 ± 0.21 kW h m^{-3}. The matrix with the highest E_{EO} was SR-NOM (7.57 ± 0.20 kW h m^{-3}) due to low pCBA

Table 3 Electrical energy per order of magnitude pCBA removal (kW h m^3) for EC:H$_2$O$_2$ operated in bicarbonate buffer. Values are the averages of duplicate experiments ± one standard deviation

| [H$_2$O$_2$]$_{initial}$/[Fe^{2+}]$_{generated}$ | Current density, mA cm^{-2} | | | | |
	3	5.5	7.4	11.1	15
0.35		0.74 ± 0.04	3.13 ± 0.13	6.10 ± 0.21	12.54 ± 2.12
0.5	0.76 ± 0.03	0.62 ± 0.02	3.15 ± 0.39	5.89 ± 0.06	
0.7		0.74 ± 0.03		7.45 ± 0.84	
1.6	1.11 ± 0.08	1.22 ± 0.05		12.56 ± 2.01	

© 2023 The Author(s). Published by the Royal Society of Chemistry

Environ. Sci.: Adv., 2023, **2**, 1574–1586 | **1583**

Table 4 Figures of merit for pCBA treatment in varying water matrices, including pseudo-first order rate constants (k) and electrical energy per order (E_{EO}) of magnitude removal values for EC:H$_2$O$_2$. For all experiments, current density = 7.4 mA cm^{-2} and H$_2$O$_2$ = 30 mg L^{-1}. pH 3 is not included due to insufficient data points to model a pseudo-first order rate constant prior to H$_2$O$_2$ depletion. pH 10.3 is not shown due to poor removal that did not provide viable data for pseudo-first order rate constants to estimate E_{EO} values

Water matrix	k, s^{-1}	E_{EO}, kW h m^{-3}
Bicarbonate buffer (pH 8.3)	1.2×10^{-3}	2.86 ± 0.20
Bicarbonate buffer (pH 6.3)	4.7×10^{-3}	0.68 ± 0.005
Bicarbonate buffer + NOM	6.3×10^{-3}	7.57 ± 0.20
Bicarbonate buffer + NOM (pH 6.3)	2.9×10^{-3}	1.13 ± 0.08
Groundwater	1.6×10^{-3}	1.00 ± 0.13
River water	1.3×10^{-3}	1.91 ± 0.21
Primary effluent	2.5×10^{-4}	6.49 ± 1.34

removal and low matrix conductivity. Primary effluent had the second highest E_{EO} of 6.49 ± 1.34 kW h m^{-3}. Notably, primary effluent had the least pCBA removal of all waters tested (<20%); however, the water's high conductivity led to low voltage input, leading to a relatively low E_{EO} in spite of the poor pCBA treatment performance.

Multivariable regressions were used to assess how water quality in environmental and synthetic water matrices influenced E_{EO}. The E_{EO} trends followed the removal trends, where DOC concentration and alkalinity increased E_{EO} by decreasing pCBA removal and increasing treatment inputs ($\beta_{DOC} = 1.2 \pm 0.15$, $p < 0.0001$; $\beta_{alkalinity} = 0.45 \pm 0.11$, $p = 0.0013$, multivariable regression: "E_{EO}, water quality"). In terms of water quality parameters, DOC$_{initial}$ had the largest negative influence on E_{EO}. For parameters that improved E_{EO}, higher water matrix conductivity improved E_{EO} by reducing the electrochemical cell's power demands ($\beta_{conductivity} = -0.29 \pm 0.1$, $p < 0.0001$, multivariable regression: "E_{EO}, water quality" ESI S10†). Accordingly, groundwater required the lowest E_{EO} of the environmental waters likely due to the low DOC concentration and high conductivity. The energy demands of the EC:H$_2$O$_2$ system operated at 7.4 mA cm^{-2} were in the range of competitive performance (*e.g.*, 1 kW h m^{-3} according to Miklos *et al.* (2018)[36]) for several water matrices (Table 4), making EC:H$_2$O$_2$ a promising option for scaled applications for treating TOrCs in environmental waters such as groundwater and river water, with the added benefit of DOC removal in the same reactor.

3.5. Conclusions

The goal of this research was to evaluate EC:H$_2$O$_2$ as a combined destructive and non-destructive treatment technology at neutral pH. This performance was assessed as a function of reactor inputs and solution pH. The treatment efficacy of environmental source waters containing varying levels of NOM, scavengers, and ionic constituents was also evaluated. Neither current density nor H$_2$O$_2$ alone promoted pCBA oxidation, although the combination of these parameters heavily influence performance. At neutral pH conditions, [H$_2$O$_2$]$_{initial}$/[Fe^{2+}]$_{generated}$ ratio was the key driver of oxidative performance,

where ratios <0.7 had higher pCBA removal and higher ratios (0.7–1.6) decreased pCBA removal, likely due to H$_2$O$_2$ scavenging.

For water quality, pH was the key driver of improved removal, where lower pH conditions minimized the competition between H$_2$O$_2$ and O$_2$ for oxidation of Fe^{2+} to better encourage radical generation. When treating groundwater and river water, EC:H$_2$O$_2$ had both oxidative treatment of TOrCs and non-destructive treatment of DOC. The pseudo-first order rate constants and E_{EO} values demonstrated that EC:H$_2$O$_2$ can be competitive with other AOPs for TOrC treatment based on energy requirements and treatment performance (depending on current density and water quality, *e.g.*, low DOC, high conductivity waters are easier to treat), with an added benefit of DOC removal due to coagulation and flocculation in the same reactor.

In real world treatment trains, EC:H$_2$O$_2$ could be operated to promote both oxidative and non-destructive treatments in a single process, which could replace multiple conventional unit processes. However, post-EC:H$_2$O$_2$ particle separation *via* sedimentation or rapid sand filtration would be needed to separate the iron flocs from solution. Additionally, a final disinfection step would likely be needed to ensure sufficient pathogen inactivation and maintain disinfectant residual. Future assessment of the performance of the full treatment train and the related energy efficiency can help to inform treatment train comparisons.

Future work is needed to evaluate EC:H$_2$O$_2$ treatment trains from a systems-engineering perspective wherein the additional benefits such as DOC removal and *in situ* chemical generation are parameterized to compare against the treatment costs associated with conventional treatment trains. These findings are needed to quantify the benefits of utilizing EC:H$_2$O$_2$ for combined treatment and provide a more comprehensive comparison of EC:H$_2$O$_2$ to current AOP technologies as well as conventional treatment trains. Additionally, the byproducts generated during EC:H$_2$O$_2$ should be evaluated. For example, the co-dissolution of regulated metals from iron electrodes (*e.g.*, manganese) could add secondary contamination. *Ex situ* H$_2$O$_2$ addition is another challenge for decentralized EC:H$_2$O$_2$ treatment. Accordingly, research is needed to inform reactor setups for EC:H$_2$O$_2$ and to explore H$_2$O$_2$ dosing technologies such as air-diffusion cathodes that can promote *in situ* H$_2$O$_2$ generation, thereby decreasing *ex situ* chemical additions and enhancing the process' potential as a small footprint decentralized treatment technology.

Author contributions

DRR: conceptualization, data curation, methodology, laboratory analyses, investigation, visualization, writing – original draft; writing – review & editing. PJM: methodology, funding acquisition, project administration, supervision, resources, validation, visualization, writing – review & editing. CKB: investigation, laboratory analysis, writing – original outline, writing – review & editing. YW: funding acquisition, resources, writing – review &editing. BKM: methodology, funding

acquisition, project administration, supervision, resources, validation, visualization, writing – review & editing.

Conflicts of interest

There are no conflicts of interest to declare.

Acknowledgements

References

1 J. C. Crittenden, R. R. Trussell, D. W. Hand, K. J. Howe and G. Tchobanoglous, *MWH's Water Treatment: Principles and Design*, 3rd edn, 2012.

2 J. J. Pignatello, E. Oliveros and A. Mackay, Advanced Oxidation Processes for Organic Contaminant Destruction Based on the Fenton Reaction and Related Chemistry, *Crit. Rev. Environ. Sci. Technol.*, 2006, **36**(1), 1–84.

3 H. J. H. Fenton, Oxidation of tartaric acid in presence of iron, *J. Chem. Soc., Trans.*, 1894, **65**, 899–910.

4 S. J. Hug and O. Leupin, Iron-catalyzed oxidation of Arsenic(III) by oxygen and by hydrogen peroxide: pH-dependent formation of oxidants in the Fenton reaction, *Environ. Sci. Technol.*, 2003, **37**, 2734–2742.

5 S. Garcia-Segura, M. M. S. G. Eiband, J. V. de Melo and C. A. Martínez-Huitle, Electrocoagulation and advanced electrocoagulation processes: A general review about the fundamentals, emerging applications and its association with other technologies, *J. Electroanal. Chem.*, 2017, **801**, 267–299.

6 A. Fischbacher, C. von Sonntag and T. C. Schmidt, Hydroxyl radical yields in the Fenton process under various pH, ligand concentrations and hydrogen peroxide/Fe(II) ratios, *Chemosphere*, 2017, **182**, 738–744.

7 F. Haber and J. Weiss, The catalytic decomposition of hydrogen peroxide Iron Salts, *Proc. R. Soc. London*, 1934, **147**, 1070–1091.

8 K. Pratap and A. T. Lemley, Fenton Electrochemical Treatment of Aqueous Atrazine and Metolachlor, *J. Agric. Food Chem.*, 1998, **46**, 3285–3291.

9 W. Stumm and G. F. Lee, Oxygenation of Ferrous Iron, *Ind. Eng. Chem.*, 1961, **53**, 143–146.

10 J. Heffron, B. McDermid and B. K. Mayer, Bacteriophage inactivation as a function of ferrous iron oxidation, *Environ. Sci.*, 2019, **5**, 1309–1317.

11 D. Lakshmanan, D. A. Clifford and G. Samanta, Ferrous and ferric ion generation during iron electrocoagulation, *Environ. Sci. Technol.*, 2009, **43**, 3853–3859.

12 K. Govindan, A. Angelin, M. Kalpana, M. Rangarajan, P. Shankar and A. Jang, Electrocoagulants Characteristics and Application of Electrocoagulation for Micropollutant Removal and Transformation Mechanism, *ACS Appl. Mater. Interfaces*, 2020, **12**, 1775–1788.

13 E. K. Maher, K. N. O'Malley, J. Heffron, J. Huo, Y. Wang, B. K. Mayer and P. J. McNamara, Removal of estrogenic compounds: Via iron electrocoagulation: Impact of water quality and assessment of removal mechanisms, *Environ. Sci.*, 2019, **5**, 956–966.

14 A. Qian, S. Yuan, S. Xie, M. Tong, P. Zhang and Y. Zheng, Oxidizing Capacity of Iron Electrocoagulation Systems for Refractory Organic Contaminant Transformation, *Environ. Sci. Technol.*, 2019, **53**, 12629–12638.

15 B. P. Chaplin, Critical review of electrochemical advanced oxidation processes for water treatment applications, *Environ. Sci.: Processes Impacts*, 2014, **16**, 1182–1203.

16 K. Pratap and A. T. Lemley, Electrochemical Peroxide Treatment of Aqueous Herbicide Solutions, *J. Agric. Food Chem.*, 1994, **42**, 209–215.

17 S. Vasudevan, An efficient removal of phenol from water by peroxi-electrocoagulation processes, *J. Water Process. Eng.*, 2014, **2**, 53–57.

18 A. R. Yazdanbakhsh, M. Kermani, S. Komasi, E. Aghayani and A. Sheikhmohammadi, Humic acid removal from aqueous solutions by peroxi- electrocoagulation process, *Environ. Health Eng. Manage. J.*, 2015, **2**, 53–58.

19 J. Behin, N. Farhadian, M. Ahmadi and M. Parvizi, Ozone assisted electrocoagulation in a rectangular internal-loop airlift reactor: Application to decolorization of acid dye, *J. Water Process. Eng.*, 2015, **8**, 171–178.

20 A. Kumar, P. V. Nidheesh and M. Suresh Kumar, Composite wastewater treatment by aerated electrocoagulation and modified peroxi-coagulation processes, *Chemosphere*, 2018, **205**, 587–593.

21 F. Ghanbari and M. Moradi, A comparative study of electrocoagulation, electrochemical Fenton, electro-Fenton and peroxi-coagulation for decolorization of real textile wastewater: Electrical energy consumption and biodegradability improvement, *Biochem. Pharmacol.*, 2015, **3**, 499–506.

22 E. Yüksel, I. A. Şengil and M. Özacar, The removal of sodium dodecyl sulfate in synthetic wastewater by peroxi-electrocoagulation method, *Chem. Eng. J.*, 2009, **152**, 347–353.

23 D. Gerrity, S. Gamage, D. Jones, G. V. Korshin, Y. Lee, A. Pisarenko, R. A. Trenholm, U. von Gunten, E. C. Wert and S. A. Snyder, Development of surrogate correlation models to predict trace organic contaminant oxidation and microbial inactivation during ozonation, *Water Res.*, 2012, **46**, 6257–6272.

24 D. R. Ryan, P. J. McNamara and B. K. Mayer, Iron-electrocoagulation as a disinfection byproduct control strategy for drinking water treatment, *Environ. Sci.*, 2020, **6**, 1116–1124.

25 E. K. Maher, K. N. O'Malley, J. Heffron, J. Huo, B. K. Mayer, Y. Wang and P. J. McNamara, Analysis of Operational Parameters, Reactor Kinetics, and Floc Characterization for

© 2023 The Author(s). Published by the Royal Society of Chemistry

Environ. Sci.: Adv., 2023, **2**, 1574–1586 | 1585

the Removal of Estrogens via Electrocoagulation, *Chemosphere*, 2018, **220**, 1141–1149.

26 Y. Pi, J. Schumacher and M. Jekel, The use of para-chlorobenzoic acid (pCBA) as an ozone/hydroxyl radical probe compound, *Ozone: Sci. Eng.*, 2006, **27**(6), 431–436.

27 E. J. Rosenfeldt, K. G. Linden, S. Canonica and U. Von Gunten, OH radical formation during ozonation and the advanced oxidation processes $O_3/H_2 O_2$ and UV/H_2O_2, *Water Res.*, 2006, **40**, 3695–3704.

28 B. J. Vanderford, F. L. Rosario-Ortiz and S. A. Snyder, Analysis of p-chlorobenzoic acid in water by liquid chromatography-tandem mass spectrometry, *J. Chromatogr. A*, 2007, **1164**, 219–223.

29 J. R. Bolton, K. G. Bircher, W. Tumas and C. A. Tolman, Figures-of-merit for the technical development and application of advanced oxidation technologies for both electric- and solar-driven systems (IUPAC Technical Report), *Pure Appl. Chem.*, 2009, **73**(4), 627–637.

30 D. Borkin, A. Némethová, G. Michaľčonok and K. Maiorov, Impact of Data Normalization on Classification Model Accuracy, *Res. Pap. – Fac. Mater. Sci. Technol., Slovak Univ. Technol.*, 2019, **27**, 79–84.

31 M. Olusegun Akinwande, H. Garba Dikko and A. Samson, Variance Inflation Factor: As a Condition for the Inclusion of Suppressor Variable(s) in Regression Analysis, *Open J. Stat.*, 2015, **5**, 754–767.

32 A. Serra-Clusellas, L. Sbardella, P. Herrero, A. Delpino-Rius, M. Riu, M. de L. Correa, A. Casadellà, N. Canela and X. Martínez-Lladó, Erythromycin abatement from water by electro-fenton and peroxyelectrocoagulation treatments, *Water*, 2021, **13**(8), 1129.

33 Environmental Protection Agency (EPA), *Enhanced Coagulation and Enhanced Precipitative Softening Guidance Manual*, 1999, EPA Office of Water, EPA 815-R-99-012.

34 L. P. Weng, L. K. Koopal, T. Hiemstra, J. C. L. Meeussen and W. H. Van Riemsdijk, Interactions of calcium and fulvic acid at the goethite-water interface, *Geochim. Cosmochim. Acta*, 2005, **69**, 325–339.

35 R. Stirling, W. S. Walker, P. Westerhoff and S. Garcia-Segura, Techno-economic analysis to identify key innovations required for electrochemical oxidation as point-of-use treatment systems, *Electrochim. Acta*, 2020, **338**(1), 135874.

36 D. B. Miklos, C. Remy, M. Jekel, K. G. Linden, J. E. Drewes and U. Hübner, Evaluation of advanced oxidation processes for water and wastewater treatment – A critical review, *Water Res.*, 2018, **139**, 118–131.

37 M. Lanzarini-Lopes, S. Garcia-Segura, K. Hristovski and P. Westerhoff, Electrical energy per order and current efficiency for electrochemical oxidation of p-chlorobenzoic acid with boron-doped diamond anode, *Chemosphere*, 2017, **188**, 304–311.